Interplay of Fe and Tm moments through the spin-reorientation transition in $TmFeO_3$

U. Staub,[1,*] L. Rettig,[1,†] E. M. Bothschafter,[1] Y. W. Windsor,[1,†] M. Ramakrishnan,[1] S. R. V. Avula,[1] J. Dreiser,[1] C. Piamonteze,[1] V. Scagnoli,[2,3] S. Mukherjee,[4] C. Niedermayer,[4] M. Medarde,[3] and E. Pomjakushina[3]

[1]*Swiss Light Source, Paul Scherrer Institut, CH-5232 Villigen PSI, Switzerland*

[2]*Laboratory for Mesoscopic Systems, Department of Materials, ETH Zurich, 8093 Zurich, Switzerland*

[3]*Laboratory for Multiscale Materials Experiments, Paul Scherrer Institut, 5232 Villigen PSI, Switzerland*

[4]*Laboratory for Neutron Scattering and Imaging, Paul Scherrer Institut, 5232 Villigen PSI, Switzerland*

(Received 26 May 2017; revised manuscript received 2 August 2017; published 7 November 2017)

X-ray magnetic circular dichroism (XMCD) and x-ray magnetic linear dichroism (XMLD) have been used to investigate the Fe magnetic response during the spin-reorientation transition (SRT) in $TmFeO_3$. Comparing the Fe XMLD results with neutron-diffraction and magnetization measurements on the same sample indicates that the SRT has an enhanced temperature range in the near surface region of approximately 82 to 120 K compared to approximately 82 to 92 K in bulk. This view is supported by complementary resonant soft x-ray-diffraction experiments at the Tm M_5 edge. These measurements find an induced magnetic moment on the Tm sites, which is well described by a dipolar mean-field model originating from the Fe moments. Even though such a model can describe the $4f$ response in the experiments, it is insufficient to describe the SRT even when considering a change in the $4f$ anisotropy. Moreover, the results of the Fe XMCD show a different temperature evolution through the SRT, the interpretation of which is hampered by additional spectral shape changes of the XCMD signal.

DOI: 10.1103/PhysRevB.96.174408

I. INTRODUCTION

Understanding coupled antiferromagnetic (AFM) systems and their magnetic phase transitions is of fundamental interest in condensed-matter physics. Transition-metal perovskites with a general formula RTO_3 can accommodate magnetic ions at both the R and the T sites. Typically, the T site is occupied by a $3d$ transition-metal ion and the R site is occupied by a $4f$ rare-earth (RE) ion. Such configuration allows magnetic superexchange interactions to exist between $3d$ transition-metal ions as well as between $3d$ transition-metal and magnetic RE ions. An archetypical example is the orthoferrite family of materials, the magnetic ordering of which has been previously studied with neutron scattering [1,2]. The magnetic structure of the Fe cage is well documented [1,3]. It has been found that some of the $REFeO_3$ exhibits a spin-reorientation transition (SRT), at which the AFM easy axis rotates by 90 deg when lowering the temperature. Due to the fact that the magnetic superexchange interaction between the well-localized $4f$ states and the $3d$ ions is much weaker than between the $3d$ ions, the superexchange between the $4f$ ions is usually neglected. Indeed, its magnetic ordering temperatures are two orders of magnitude lower than that of the Fe sublattice. However, the SRT occurs only in $REFeO_3$ perovskites in which the RE ion is a magnetic $4f$ ion, and the transition temperature varies dramatically for materials with different RE ions. For instance, Sm has the SRT above room temperature, whereas for Tm it is around 85 K and for Yb it is around 10 K [4]. This indicates that the magnetic state of the RE ion plays a role in the SRT, though very little is known about the role of the RE ions' magnetic state in the vicinity of the transition [5].

Recent years have seen renewed interest in orthoferrites, as their magnetic SRT behavior may open new directions in the field of spintronics, with the goal of increasing the speed of magnetic recording well below the nanosecond regime. The focus has been on ultrafast manipulation of magnetic order, achieved by exciting the system with ultrashort and intense optical pulses [6–8]. It has indeed been shown that a significant spin reorientation can be obtained on ultrafast time scales in $TmFeO_3$ [6]. Inducing the SRT with an ultrashort laser pulse also leads to coherent magnetic excitations represented by a coherent modulation of the magnetization. Even more interesting is that such magnetic excitation can be excited directly by momentum transfer from circular polarized optical pulses, which constitutes the first observation of the inverse Faraday effect [7]. More recently, it has been proposed that exciting two optical phonon modes with a controlled relative phase can mimic a magnetic field and result in an excitation of the spin system [9].

$TmFeO_3$ crystallizes in *Pbnm* symmetry and orders antiferromagnetically far above room temperatures, containing four chemical formula units in the unit cell that is approximately $\sqrt{2}a_p \times \sqrt{2}a_p \times 2a_p$, with a_p the cubic perovskite lattice constant. The Fe magnetic sublattice orders at $T_N \sim 632$ K [10] in a simple G-type structure. Fe moments are antiferromagnetically ordered (staggered M_{AF}) pointing along the a axis for temperatures above the SRT, whereas at temperatures below the SRT the moments point along the c axis [1]. Cooling through the SRT is characterized by an onset temperature $T_2 \sim 92.8$ K at which the spins start to coherently rotate away from $M_{AF}//a$, and an end temperature $T_1 \sim 82.5$ K at which all spins have reached their final direction $M_{AF}//c$ (see Fig. 1). In addition to the simple AFM structure, there is a small spin canting caused by the Dzyaloshinskii-Moriya (DM) interaction that induces a weak ferromagnetic (FM)

*urs.staub@psi.ch

†Present address: Department of Physical Chemistry, Fritz-Haber-Institut of the Max Planck Society, Faradayweg 4-6, Berlin 14915, Germany.

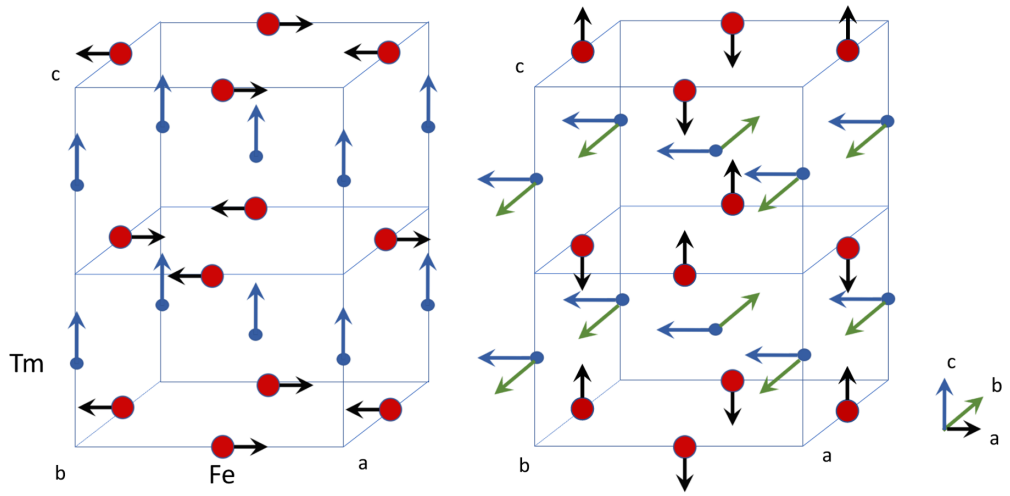

FIG. 1. Sketch of the magnetic structure of $TmFeO_3$ and the corresponding dipolar magnetic field components at the Tm site. The latter represent also the induced Tm moments (right, $T < T_1 = 82.5$ K; left, $T > T_2 = 92.8$ K [2]), as for paramagnetic Tm the moments have to follow the effective field direction.

moment M_F. This moment rotates also coherently in the same $a-c$ plane, for decreasing temperatures from $M_F//c$ to $M_F//a$ through the SRT, remaining perpendicular to M_{AF} at these temperatures. An additional weak AFM spin canting is allowed by symmetry [4]. As it is on the order of 1.6% [11] of the total moment we do not consider this canting further here. The strong dependence of the SRT on the $4f$ electron system, which itself does not magnetically order above 4 K, has led to the general belief that the SRT is initiated by the strong $4f$ magnetic anisotropy associated to the large orbital magnetic moment and can vary strongly via thermal occupancy changes in the $4f$ orbital levels. As the Fe^{3+} ion in the orthoferrites has a half-filled shell that exhibits only a small magnetic single-ion anisotropy, very small external forces such as the weak magnetic interaction between the $4f$-$3d$ shells can influence its spin easy axis.

Resonant x-ray techniques are powerful tools to investigate magnetic properties of materials [12], in particular due to their element selectivity, which allows us to follow FM and AFM atomic moments for the different elements separately. For $3d$ transition-metal ions these techniques are very sensitive in the soft-x-ray regime and a number of different coupled magnetic transition-metal oxide systems have been already studied in the past by both XMCD and resonant x-ray-diffraction techniques [13–17]. In orthoferrites, XMCD and XMLD have been used to characterize the magnetic ordering phenomena of the Fe sublattice, or its interaction with other magnetic layers grown on it [18–22].

In this paper, we discuss resonant x-ray diffraction at the Tm M_5 edge to study the magnetic structure and orbital orientation of the Tm ions through the SRT. Our results show that the Fe^{3+} spins induce an antiferromagnetic component on the Tm ions only below the onset temperature of the SRT. This is compared to a dipolar mean-field calculation. In addition, XMLD and XMCD at the Fe $L_{2,3}$ edges in reflection geometry are presented. XMLD is a measure of $\langle M^2 \rangle$, and therefore only sensitive to the uniaxial direction of the magnetic moment and therefore dominated by the large moment of the AFM subsystem. For more details see, e.g., [23–25]. XMCD is sensitive to the FM Fe components, respectively. These results show that the surface of our polished crystal has a much wider SRT than the bulk, which is visible in the XMLD of the Fe and Tm magnetic scattering, both probing the AFM component. The weak FM signal exhibits a different temperature dependence and is more difficult to analyze due to additional changes of spectral shape of the signal.

II. EXPERIMENTS

Polycrystalline $TmFeO_3$ was prepared by a solid-state reaction. Starting materials of Tm_2O_3 and Fe_2O_3 with 99.99% purity were mixed and ground followed by heat treatment at 1000–1250 °C in air for a duration of 70 h with several intermediate grindings. Phase purity of the compound was checked with a conventional x-ray diffractometer. The resulting powder was hydrostatically pressed in the form of rods (7 mm in diameter and ~60 mm in length). The rods were subsequently sintered at 1300 °C for 20 h.

The crystal growth was carried out using an optical floating zone furnace (FZ-T-10000-H-IV-VP-PC, Crystal System Corp., Japan). The growth conditions were the following: growth rate was 5 mm/h, both rods (feeding and seeding rod) were rotated at about 20 rpm in opposite directions to secure the liquid homogeneity, and 1.5 bars of pressure of an oxygen and argon mixture were applied during the growth process.

The crystal was oriented by Laue diffraction and different pieces cut along the [011], [100], and [001] directions. The surface was polished and annealed at 800 °C for 20 h in oxygen flow. Magnetization measurements were conducted using a commercial magnetic property measurement system superconducting quantum interference device magnetometer.

The resonant x-ray-scattering experiments were conducted using the RESOXS ultrahigh-vacuum diffraction end station [26] at the surface and interface microscopy (SIM) beamline [27] of the Swiss Light Source. Linearly polarized incident light with either π or σ polarization (electric field in the scattering plane or perpendicular to it, respectively) was used for the resonant diffraction experiments of the (011) reflection

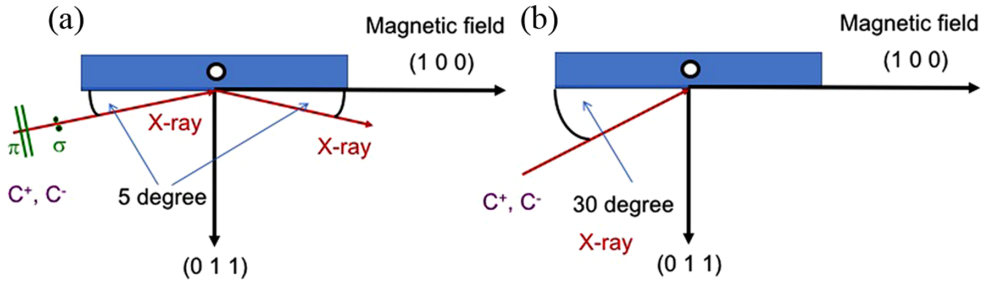

FIG. 2. Sketch of the (a) XMCD and XMLD scattering geometry in reflection geometry and (b) XMCD taken in total electron yield mode. The polarization of the x rays is given by $c+$ and $c-$ for circular polarizations and σ and π for the linear polarizations. Note that experiments have been taken in remanence.

at the Tm M_5 edge, and for the XMLD experiments at the Fe $L_{2,3}$ edges performed in reflection geometry. Circularly polarized light with opposite handedness was used for the XMCD experiments at the Fe $L_{2,3}$ edges in reflection geometry [28]. For all measurements below the SRT, the sample was cooled through the SRT in a magnetic field of 0.1 T pointing along the a axis to obtain a single magnetic domain state. This field was created by a permanent magnet that was removed before the measurements. Additional XMCD and XMLD experiments were performed at the X-Treme beamline [29] in total electron yield mode. This is done via a measurement of the drain current onto the sample, which brings back the electrons lost by the photoeffect. This signal is proportional to the x-ray absorption. For these experiments, the samples were covered with a 2–3-nm-thick conducting carbon layer to reduce charging, which could not be fully suppressed, limiting the data quality. Finally, neutron-diffraction experiments were performed at the cold neutron triple-axis spectrometer RITA-II, SINQ, Paul Scherrer Institut using an incident wavelength of $\lambda = 4.21$ Å from a pyrolytic graphite (002) monochromator and a 80' collimation between monochromator and sample. A pyrolytic graphite filter between monochromator and sample and a cooled Be filter between sample and analyzer reduced higher-order contaminations of the incident beam. The sample was mounted in an orange cryostat with the (001) and (100) directions in the scattering plane.

III. RESULTS

A. Fe magnetic subsystems

To study the FM Fe spin components, reflectivity spectra at 5-deg incidence were collected at 10 K for opposite circular light polarization in the vicinity of the Fe $L_{2,3}$ edges. The sample surface out-of-plane axis was (011), and for a 0-deg x-ray gracing incidence angle the incoming beam would have been parallel to the a axis (see Fig. 2). These are shown in Figs. 3(a) and 3(b) for positive and negative field cooling through the SRT, respectively. Figures 3(c) and 3(d) show the corresponding XMCD response. Opposite XMCD signals are observed for opposite field cooling cycles indicating that the response is indeed magnetic in origin. A well-defined XMCD contrast is observed at the L_2 edge around 723.5 eV.

X-ray reflectivity spectra with π and σ incident polarization obtained at 10 K, taken in the same geometry as the XMCD data [Fig. 3(a)], and the corresponding XMLD contrast [Fig. 3(b)] provide information about the AFM Fe order. Significant XMLD contrast is observed at both edges, as is expected from previous XMLD experiments on $LaFeO_3$

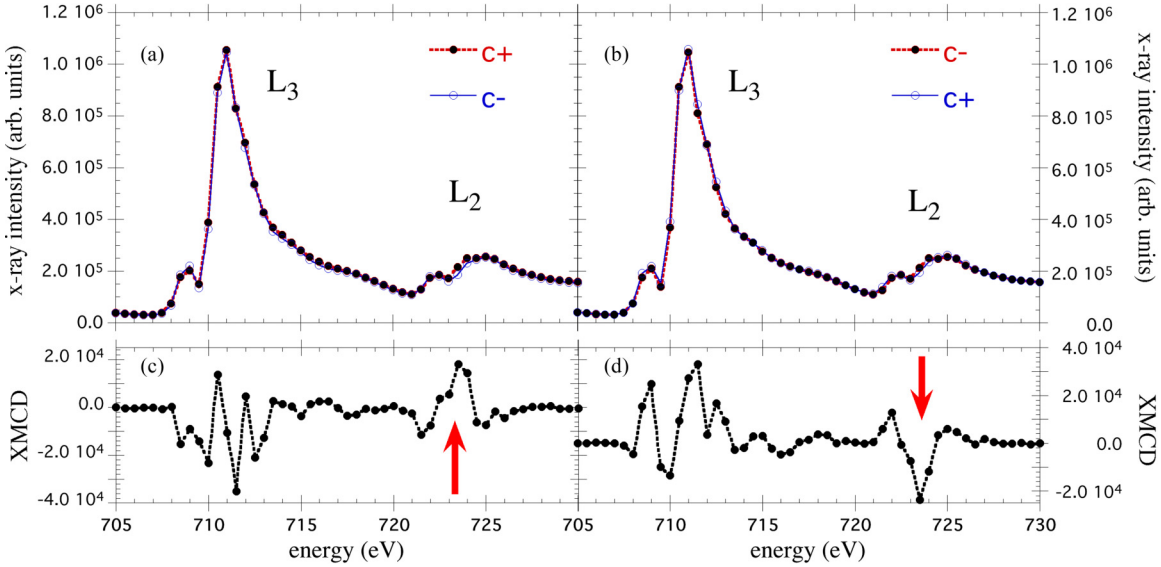

FIG. 3. Photonenergy dependence of the x-ray reflectivity taken with opposite circular light polarization and its XMCD signals for (a), (c) positive field (H+) and (b), (d) negative (H-) field cooling.

[18]. Maximal contrast is observed at 711.5 eV, where further temperature-dependence measurements were performed. No differences have been found for opposite magnetic field cooling within experimental accuracy, as expected for an antiferromagnetic XMLD signal (not shown).

To study the Fe magnetic response through the SRT, the temperature-dependent XMCD $(I_+ - I_-)/(I_+ + I_-)$ and XMLD $(I_\sigma - I_\pi)/(I_\pi + I_\sigma)$ asymmetries were collected at the energies with optimal contrast. These are shown in Figs. 4(a) and 4(b). Note that as the XMCD and XMLD signals are a measure of different multipole moments they have different spectral shapes. For increasing temperatures, the XMCD and XMLD asymmetries start to vary around the onset of the bulk SRT temperature ($T_1 \approx 82$ K). The XMCD asymmetry shows an extremum around 100 K. The XMLD shows a change of slope at T_1; however, it is followed by a linear temperature dependence up to approximately 120 K, where a second kink indicates that the AFM contribution of the SRT transition is completed (T_2). The corresponding transition temperature T_2 from literature [2,4] ($T_2 \approx 92$ K) is shown as a dotted line in Fig. 5. Similar XMLD temperature dependence is also obtained for having the a axis perpendicular to the scattering plane. Our results are clearly not compatible with T_2 from literature. This can be due to the fact either that our $TmFeO_3$ crystal has different magnetic properties compared to previously published bulk samples or that the surface behaves differently. Note that extended SRT ranges have already been mentioned to be possibly related to the employed experimental technique [30].

The probe depth of the XMCD and XMLD asymmetries taken in reflection geometry at these low incident angles is approximately 5 nm at resonance, making their response surface sensitive.

To test the bulk magnetic properties, we performed magnetization measurements on the same crystal for magnetic fields along the (100) and (001) directions, which are shown in Fig. 6. These data show that the bulk FM moments of the crystal exhibit T_1 and T_2 transition temperatures that

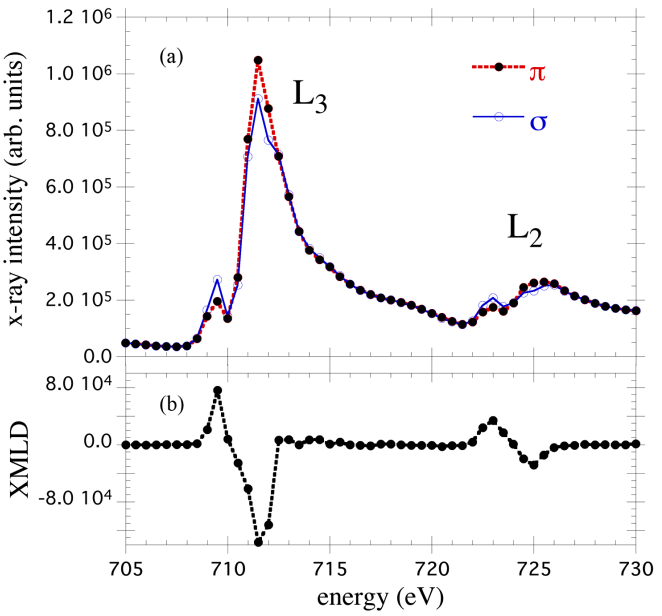

FIG. 4. (a) Photonenergy dependence of the x-ray reflectivity taken at 5-deg incidence angle for π and σ incident polarization and (b) its corresponding XMLD signal.

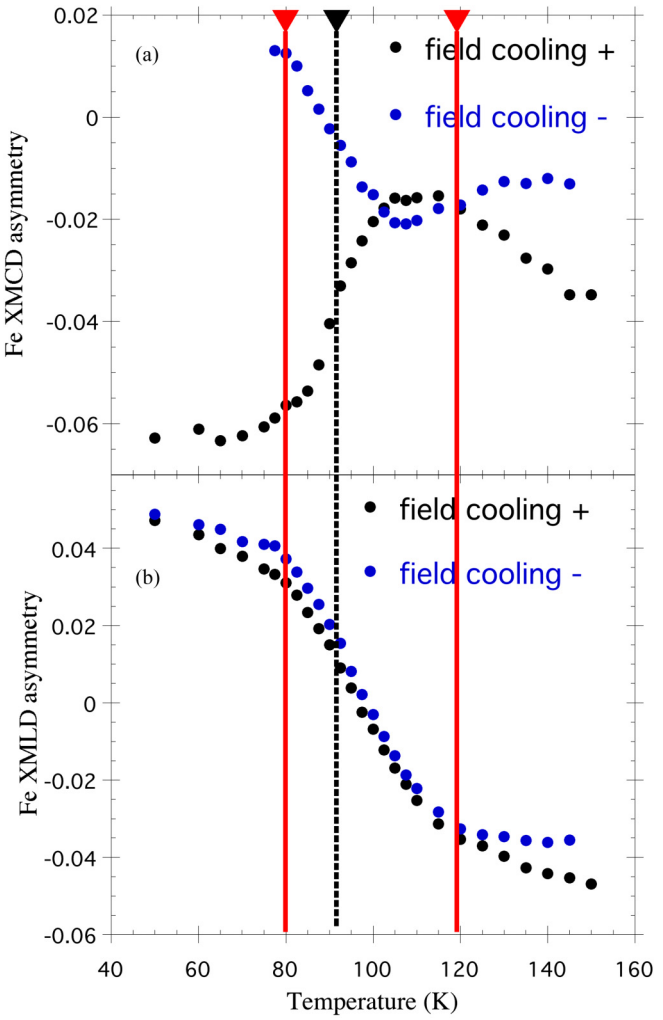

FIG. 5. Temperature dependence of the XMCD and XMLD asymmetries measured in reflection for opposite field cooling. The red solid line shows lower and higher transition temperature T_1 and T_2 of the SRT, respectively, whereas the dashed black line shows the higher transition temperature for the published bulk data [4].

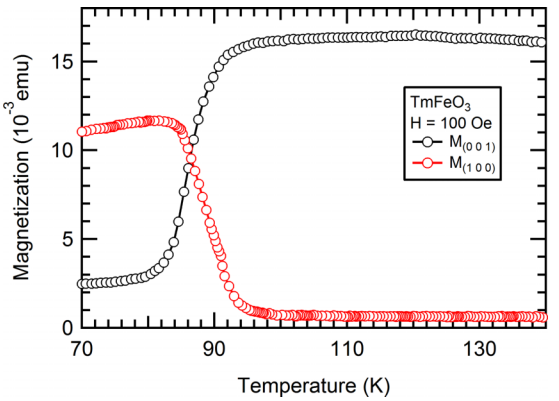

FIG. 6. Temperature dependence of magnetization along the [001] and [100] directions of a single crystal of $TmFeO_3$.

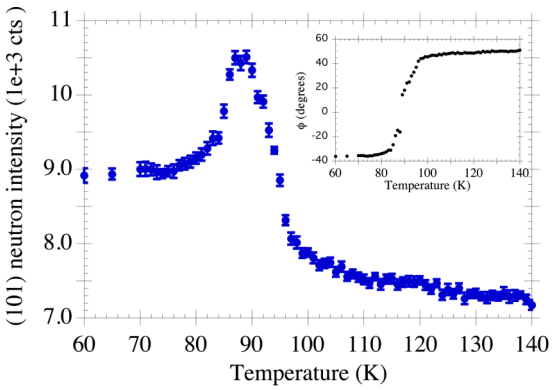

FIG. 7. Temperature-dependent neutron-scattering intensity of the (101) reflection of $TmFeO_3$ containing both structural and magnetic components. Inset: Calculated rotation angle with respect to the momentum transfer (101) of the AFM Fe spin component extracted from the reflection intensities.

are consistent with those reported in literature. Note that any possible spin polarization at the Tm site at elevated temperatures is much weaker than the Fe moments, so the measured magnetization represents mostly the FM Fe spin canting. However, above bulk $T_2 \approx 92$ K there is still a slight increase in magnetization observed for increasing temperatures, peaking around 120 K, at the same temperature at which the XMLD asymmetry changes slope. The AFM bulk properties were tested by collecting the neutron-diffraction intensity from the (101) reflection in zero applied field. The intensity has both a structural and a magnetic scattering contribution. The AFM axis can rotate either through the [101] or [10–1] direction when rotating from the [001] to the [100] direction during the SRT. The temperature dependence, shown in Fig. 7, allows us to distinguish between the two cases. It exhibits a distinct increase in neutron-scattering signal through the SRT. This indicates that a majority of the domains rotate through the (10-1) direction, because the signal (the neutron-scattering cross section chapter 7 of Ref. [29]) is sensitive to the magnetic moments perpendicular to the momentum transfer wave vector [$\mathbf{Q}\|(101)$] [31]. Assuming that the temperature-dependent intensity is caused by such a majority domain rotation and assuming at 50 K $\mathbf{M}_{AF}//(001)$ and at 140 K $\mathbf{M}_{AF}//(100)$ results in a smooth rotation of the spin direction, which is visualized in the inset of Fig. 7. These results are consistent with the FM moments observed in the magnetization measurements, which indicate that the bulk FM moments remain pinned perpendicular to the AFM moments through the SRT. These bulk results clearly indicate that our $TmFeO_3$ crystal has the main magnetic properties as reported previously and that it is the surface regions that cause the difference in the XMCD and XMLD. The surface has a much higher T_2 and an extended SRT temperature range.

To confirm such a scenario, and in particular to understand the unexpected behavior of the XMCD asymmetry taken in grazing incidence, standard XMCD measurements in total electron yield mode would be very helpful. However, due to the strong insulating character of the crystals, charging effects are too large to obtain reasonable XAS and XMCD spectra from the surface region in standard electron yield mode. To

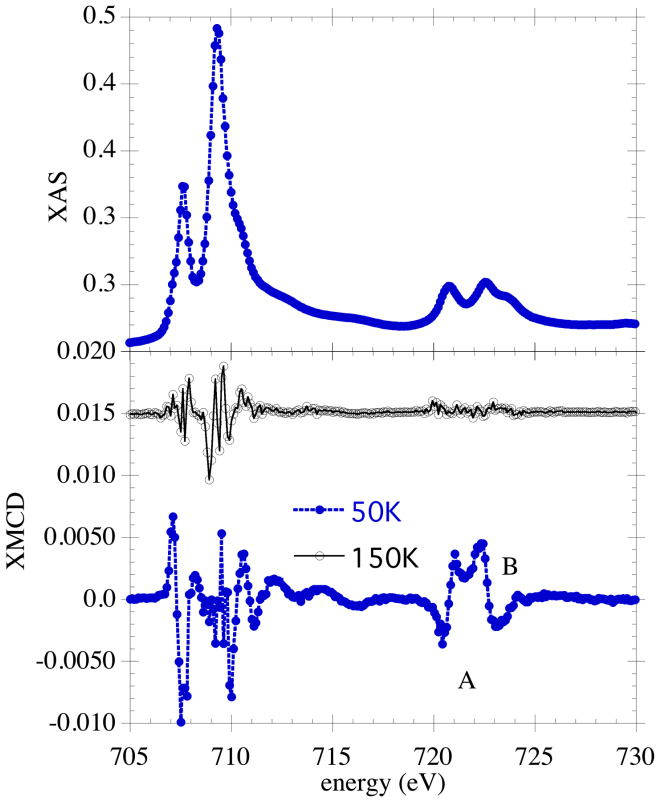

FIG. 8. XAS (upper panel) at $T = 50$ K and XMCD spectra (lower panel) of $TmFeO_3$ in the vicinity of the Fe $L_{2,3}$ edges at two different temperatures measured by total electron yield. The curves are offset for clarity. A and B represent the spectral features at which the temperature dependence has been taken.

reduce the effect of charging, the sample was coated by 2–3 nm of carbon. Carbon coating of an oxide is relatively gentle and is expected not to significantly change the probed properties. Figure 8 shows the XMCD spectra with the incoming x-ray beam at 30 deg to the (100) axis taken from a [011] surface cut of the crystal (see Fig. 2). The sample was cooled in a magnetic field applied along the x-ray beam direction prior to the measurement. The XMCD data at the L_3 edge are still significantly affected by charging and only the data at the L_2 edge are sufficiently smooth to be dominated by the intrinsic XMCD. This is confirmed by the absence of a clear XMCD at 150 K, as expected when the FM Fe moment is expected to be close to perpendicular to the incoming x-ray direction.

The temperature dependences of the average XMCD signal in region A (720.8 to 722.6 eV) and region B (722.7 to 724eV) are shown in Fig. 9. These data exhibit a crossing of the XMCD asymmetries at 103 K and another possible cancelation at 120 K. The same feature was observed in the temperature dependence of the reflectivity in Fig. 5(a). To test the origin of this crossover, it is important to look at the spectral shape at these temperatures. As this XMCD signal is very weak, we averaged the XMCD spectral shape in the temperature range 107.5–112.5 K, which is shown in the inset of Fig. 9. The shape shows distinct changes compared to that taken at 50 K indicating that the crossing does not come from a cancellation of magnetic moments along the probe

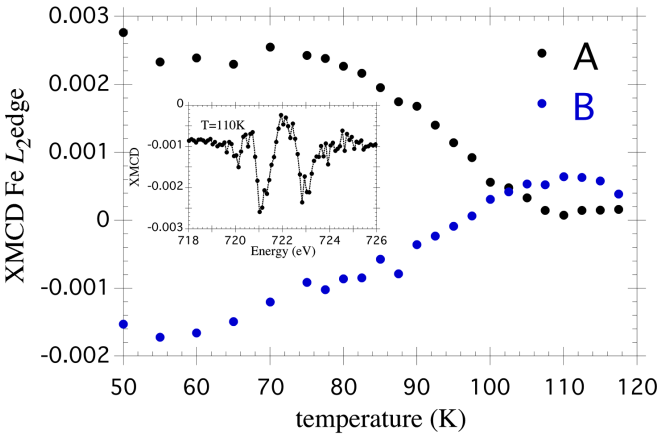

FIG. 9. Temperature dependence of the averaged XMCD signal of spectral range A (720.8–722.6 eV) and B (722.7–724eV) measured by total electron yield. Inset: Spectral shape of the XMCD signal averaged in the temperature range 107.5–112.5 K, showing differences in spectral shape compared to that found at 50 K (Fig. 2).

direction, but is rather due to differences from XMCD signals for different FM moment directions in the crystal.

B. Tm 4*f* magnetism

The energy dependence around the Tm M_5 edge of the (011) reflection for opposite field cooling is shown in Fig. 10 for σ and π incoming linearly polarized x rays. The sample was at an azimuthal angle $\Psi = 180^\circ$, which corresponds to the *a* axis in the scattering plane. Thomson scattering is symmetry forbidden for the (011) reflection in *Pbnm* symmetry. However, the aspherical charge distributions of the resonant ions (Tm) have different orbital alignments at the four crystallographically equivalent 4*c* sites, which allows resonant scattering for this reflection. The individual Tm ions have different local crystal-field axis orientations, which are directly related to the tilts of the oxygen octahedra. Therefore, the resonant scattering cross section in the electric dipole-dipole approximation for this reflection at the M_5 edge ($3d$ to $4f$ transition) is sensitive to the quadrupole electron density in the $4f$ shell. Because there are four Tm ions per cell, only the antiferro-type *quadrupole (orbital) orientation* contributes to the intensity. The temperature dependence of the expectation value of the ordered quadrupole(s) is dominated by the occupancy of the relevant low-lying $4f$ states, which follow Boltzmann statistics. Tm $4f$ quadrupoles have also been observed at the Tm M_5 edge in isostructural $TmMnO_3$, where the forbidden (010) reflection was investigated [17,32].

The energy scans of the (011) reflection taken at 10 K for opposite field cooling differ significantly from each other [positive field cooling, Fig. 10(a), and negative field cooling, Fig. 10(b)]. This is also clearly visible in the corresponding asymmetry $(I_\pi - I_\sigma)/(I_\pi + I_\sigma)$, which shows maxima/minima just before the main M_5 resonance [Fig. 10(c)]. This indicates that the diffraction intensity is not purely from the antiferro order of the $4f$ quadrupoles but contains an additional magnetic contribution that is magnetic field dependent. This weak magnetic signal interferes in the structure factor having opposite phase for the magnetic scattering amplitude for opposite AFM domains. As the FM and AFM domains are coupled, the applied magnetic field creates a single AFM domain state. The intensity (structure factor squared) therefore differs for opposite magnetic fields. At 100 K, the (011) reflection is much weaker at resonance than at lower temperatures. This is a direct consequence of the depopulation of the $4f$ ground state that reduces the asphericity of the $4f$ electron density. In addition, the intensity difference for opposite magnetic field cooling is also strongly reduced, resulting in a very small asymmetry for linear polarization. It shows that the magnetic contribution has almost vanished at this temperature. A magnetic contribution is also observed when laterally scanning the sample surface in the (011) Bragg condition. A spatially homogeneous magnetic signal is observed when the sample is field cooled (not shown), as expected in a single-domain state. A different result is expected in the presence of magnetic domains. Figure 11 presents such a scan at 40 K, without prior field cooling. Clear contrast is observed between antiferromagnetic domains that are several hundred micrometers wide and up to 2–3 mm in length. This contrast disappears when heating the crystal to 170 K, demonstrating the absence of a magnetic signal at this temperature.

To study the magnetic response of the Tm $4f$ system through the SRT, we follow the integrated intensity of the (011) reflection for increasing temperatures for σ and π polarization at the energy of the Tm M_5 edge with maximal magnetic contrast (1457 eV) and with maximal orbital (quadrupole) intensity (1459.2 eV). The intensity ratio between the two polarizations is shown in Fig. 12 as a function of temperature for both energies and opposite field cooling directions. The magnetic contrast (solid symbols) strongly decreases upon warming, and is no longer detectable above $T \approx 120$ K, which coincides with T_2 obtained from the Fe XMLD signal. The magnetic contribution (open symbols) shows a much weaker contrast at the main orbital resonance energy. The temperature dependence of the magnetic signal shows a typical mean-field-like induced behavior for $4f$ magnetic moments similar to that found in $NdNiO_3$ [13] or $TmMnO_3$ [17]. In isostructural $TmMnO_3$ the Tm ions are at the same crystallographic site with a similar crystal-field potential. In addition, the Fe and Mn are both trivalent, leading to a similar crystal-field potential at the Tm site, allowing a comparison of spectral shapes between the two materials. It will be shown later that the same quadrupole is observed at the (010) and the (011) reflections in these systems, resulting in an indeed similar spectral shape for these reflections. For the spectral shape of the magnetic scattering, the similarity is expected to be even larger, as the crystal-field splitting of the $4f$ states of a few tens of meV is generally much smaller than the multiplet structure of a few eV at the M_5 edge. This leads also to very little variation in $4f$ M_5 edge XMCD spectra for materials, which contain the same trivalent $4f$ ions. The energy spectra reported in Ref. [17] for $TmMnO_3$ indicate that the magnetic scattering signal is maximal at a slightly lower energy than the maxima of the orbital scattering. This is in agreement with our data, and further supports the magnetic origin of the signal at 1457 eV in our $TmFeO_3$ system.

To study the spatial symmetry of the quadrupolar order on Tm, we collected its azimuthal angle dependence (rotation

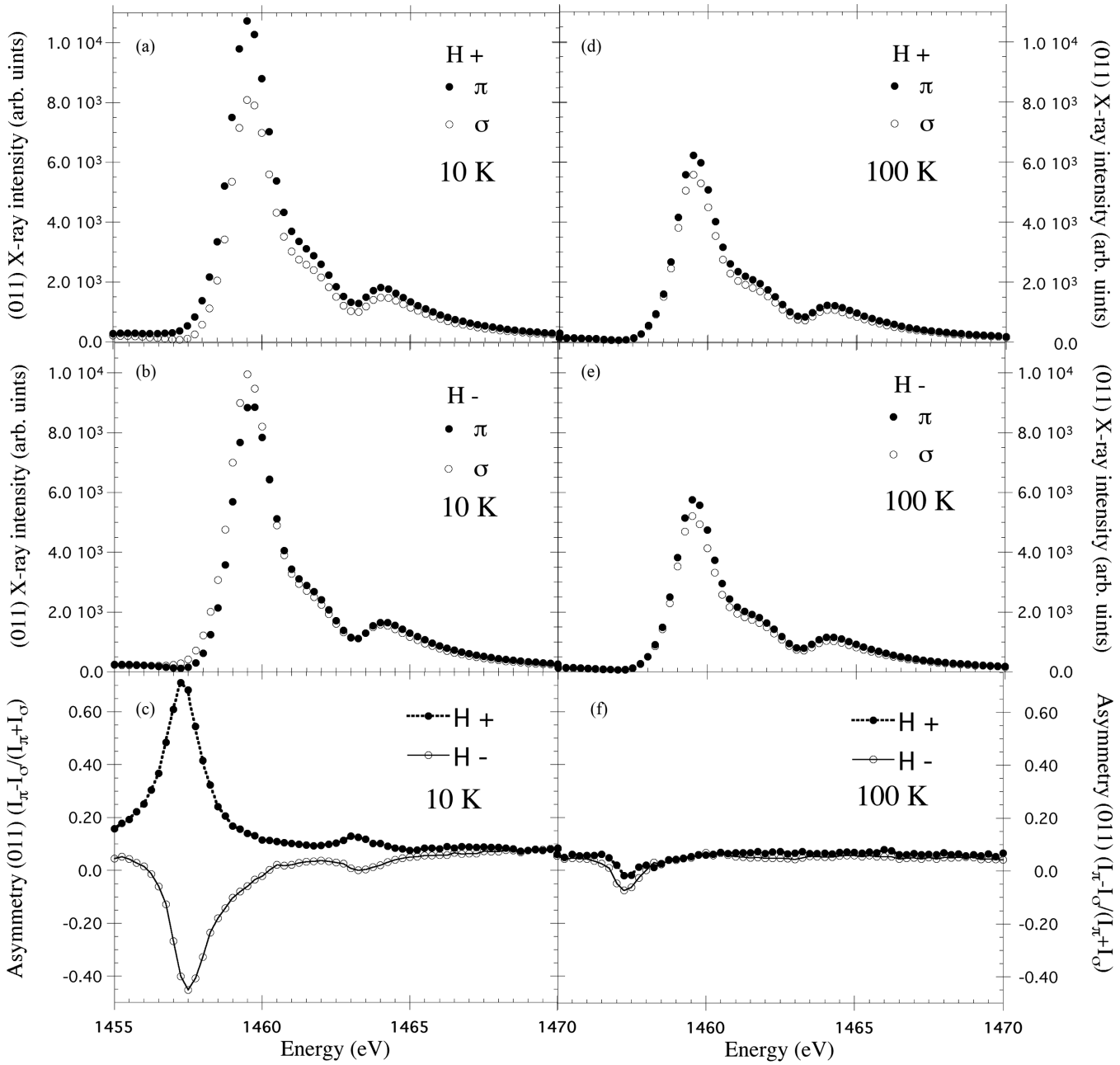

FIG. 10. Photoenergy dependence of the (011) reflection in the vicinity of the Tm M_5 edge of $TmFeO_3$ for incident σ and π polarized x rays for $\Psi = 180^\circ$, taken at (a)–(c) $T = 10$ and (d)–(f) 100 K, for opposite field cooling and its corresponding asymmetries. (a) and (c) Positive field cooling, (b) and (e) negative field cooling, and (c) and (f) corresponding asymmetries taken at 10 K.

about the scattering vector) in the low-temperature phase at the maxima of the M_5 edge diffraction spectrum, which is shown in Fig. 13.

Following Lovesey *et al.* [33], the resonant unit-cell structure factor for the (011) reflection (with momentum **Q**) without the magnetic contributions can be written as

$$\Psi_Q^K = \sum\nolimits_d e^{i\mathbf{Qd}} \langle \mathrm{T}_Q^2 \rangle_d \tag{1}$$

for which $\langle \mathrm{T}_Q^2 \rangle$ is a Tm $4f$ quadrupole with projection Q (spherical coordinate system). The sum goes over all the Tm sites with individual positions **d**. Tm occupies the Wyckoff position $4c$ that has a $-m$ symmetry, which implies $\langle \mathrm{T}_Q^2 \rangle = (-1)^Q \langle \mathrm{T}_Q^2 \rangle$. This constrains $\langle \mathrm{T}_Q^2 \rangle$ to be zero for $Q = 1$ or -1 and it follows that the sum over the four Tm positions in the cell leads to

$$\Psi_2^2 = -\Psi_{-2}^2 = -4i \sin(2\pi y) \langle \mathrm{T}_2^2 \rangle'', \tag{2a}$$

$$\Psi_1^2 = \Psi_{-1}^2 = \Psi_0^2 = 0, \tag{2b}$$

with y the fractional atom position of the Tm ion. The unit-cell structure factor has to be implemented into the scattering geometry to obtain the "global" structure factor and the corresponding intensity as a function of the azimuthal angle. For this we evaluate the quantities A_Q^K and B_Q^K

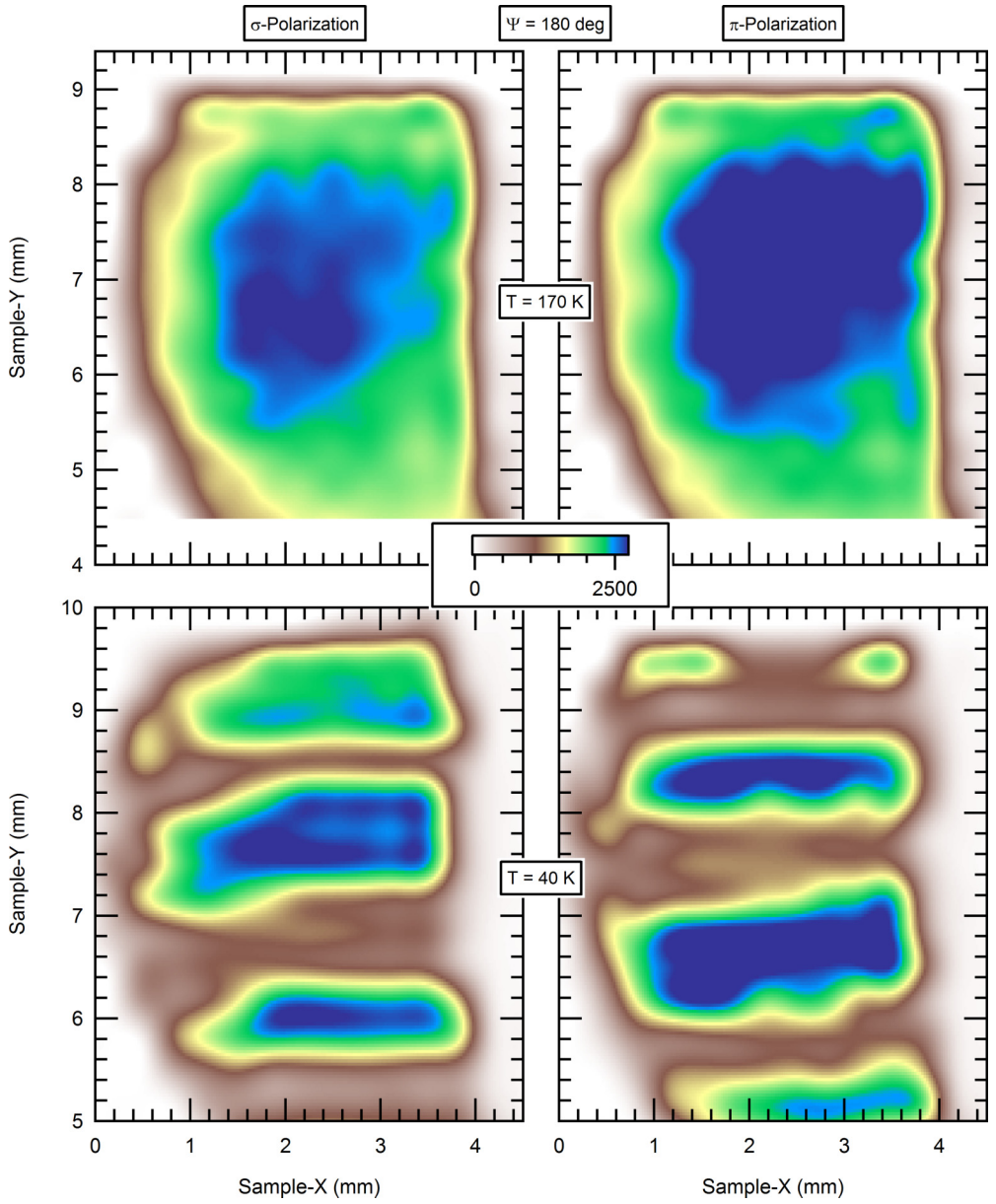

FIG. 11. Intensity of the (011) reflection as a function of beam position on the sample, measured at 1457.2 eV (maximum magnetic contrast) in the vicinity of the Tm M_5 edge of $TmFeO_3$ for incident σ and π polarization taken at $T = 40$ (lower panels) and 170 K (upper panels). The data at $T = 40$ K are taken without field cooling and show the breakup in opposite AFM domains.

defined in Eqs. (B2) and (B3) of Ref. [34] and obtain only two nonzero elements $A_1^2 = 4i\sin(\gamma)\sin(2\pi y)\langle T_2^2\rangle''$ and $B_2^2 = 4i\cos(\gamma)\sin(2\pi y)\langle T_2^2\rangle''$, from which we can obtain the structure factor for the different polarization channels as outlined in Appendix C of Ref. [34]. It results in

$$F_{\sigma'-\sigma} = 4\sin(2\psi)\sin(\gamma)\sin(2\pi y)\left\langle T_2^2\right\rangle'', \quad (3a)$$

$$F_{\pi'-\sigma} = 4[\cos(2\psi)\sin(\theta)\sin(\gamma) - \sin(\psi)\cos(\theta)\cos(\gamma)]\sin(2\pi y)\left\langle T_2^2\right\rangle'', \quad (3b)$$

$$F_{\sigma'-\pi} = -4[\cos(2\psi)\sin(\theta)\sin(\gamma) + \sin(\psi)\cos(\theta)\cos(\gamma)]\sin(2\pi y)\left\langle T_2^2\right\rangle'', \quad (3c)$$

$$F_{\pi'-\pi} = 4\sin(2\psi)\sin^2(\theta)\sin(\gamma)\sin(2\pi y)\left\langle T_2^2\right\rangle'' \quad (3d)$$

with θ the Bragg angle of the (011) reflection, $\langle T_2^2\rangle''$ the imaginary part of the $\langle T_2^2\rangle$ quadrupole, and $\gamma = a\tan(bl/ck)$, where b and c are the lattice constants, and k and l are the Miller indices of the reflection. The corresponding azimuthal dependence is shown in Fig. 13 and is in excellent agreement with the data. It shows that the reflection is indeed well described by a single $4f$ quadrupole contribution, with small deviations caused by the small magnetic contribution at this energy. Note that the calculation of the resonant scattering structure factor of the space-group forbidden (010) reflection results in the same single quadrupole component contribution. The rotated light channels are again proportional to $\langle T_2^2\rangle''$, whereas there is no quadrupolar contribution for the unrotated light polarization channels. This shows that indeed both reflections, the (010) and (011), are expected to have the same spectral shape.

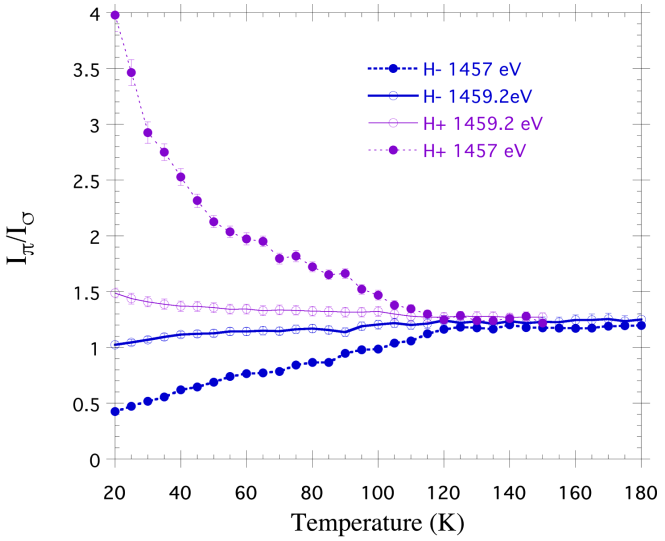

FIG. 12. Temperature dependence of the (011) intensity ratio of σ and π polarization for cooling in opposite fields taken at the energy of maximum contrast (1457 eV) and at the maximum of the spectral shape intensity (1459.2 eV). All data are taken in the vicinity of the Tm M_5 edge.

IV. DISCUSSION

The SRT in orthoferrites depends strongly on the $4f$ magnetic anisotropy. It is therefore interesting to study the interaction between the $4f$ and $3d$ moments that mediates the anisotropy between the two sublattices. The simplest approximation to describe the exchange interaction between the two magnetic subsystems is a mean-field approach, in which the strongly coupled Fe moments lead to a net magnetic field at the paramagnetic Tm site. The very low magnetic ordering temperature of the Tm sublattice typical for oxides reflects the very well-localized $4f$ electron density, and the corresponding weak superexchange interactions through the bridging oxygen support such a simple assumption. As such, the effective field at the Tm site can be modeled using the magnetic dipole interaction, which successfully described the induced Tm moment that was extracted from azimuthal angle scans of resonant soft-x-ray diffraction at several reflections in $TmMnO_3$ [17]. Following such a promising starting point, we calculated the mean field created by the Fe moments at the Tm site as in Ref. [17]. Here we assume that the Fe moments are along the main crystallographic axis, as the canting from the weak DM interaction is small. The resulting mean field from the Fe AFM moments along the a axis for $T > T_2$ produces a single FM component at the Tm site pointing along the c axis. This induced Tm moment enhances the FM spin component from the Fe canting. Note that also for $TmMnO_3$ the induced Tm moment was found to be perpendicular to the Mn moment, though the magnetic structure of the Mn sublattice is different [17]. The calculations for the magnetic phase with $T < T_1$ predict two different mean-field components on the Tm, originating from the c-axis oriented AFM Fe moments: an AFM component along the b axis and a FM component along the a axis. The latter will further add to the Fe a-axis spin canting producing the overall bulk magnetization. This induced FM moment has the same magnitude as the one for $T > T_2$ (in comparison to the inducing Fe moment). This Tm moment is expected to be larger in the low-temperature phase as the single-ion "paramagnetic" susceptibility is strongly temperature dependent. The AFM mean-field component points along the b axis and is approximately five times larger than the FM component. The induced $4f$ moment from this component will lead to a magnetic scattering signal at the (011) reflection, which is consistent with our observation.

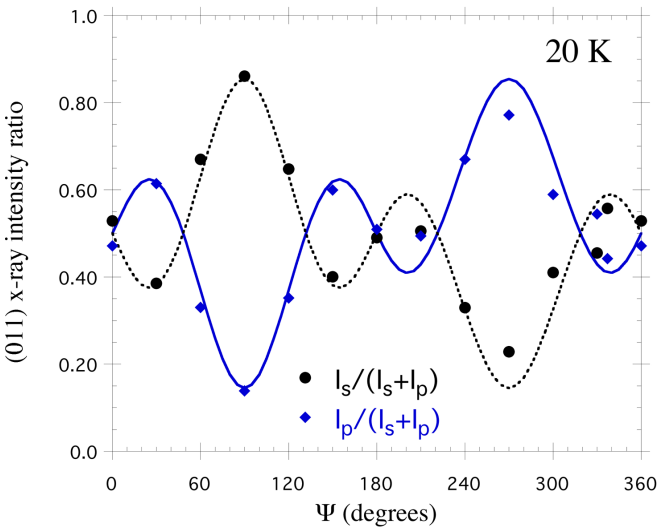

FIG. 13. Azimuthal angle dependence of the intensity normalized σ and π polarized (011) reflection intensities taken at 20 K at the maxima of the spectra. The lines are calculations as explained in the main text.

The temperature dependence of the induced $4f$ moment can be described by the temperature dependence of the effective field on the Tm site created by the Fe moments (J_{3d-4f}) and the response of the Tm ions to it. The response is described by the paramagnetic single-ion susceptibility of the Tm ion along the effective mean-field direction, which follows a Curie-Weiss-like $1/T$ behavior over a wider temperature range. As the angle of rotation of the Fe spins from $\alpha = 0$ to 90 deg is roughly linear between T_1 and T_2, (supported by XMLD data, neutron data, and magnetization data) the field will be proportional to $\sin(\alpha)$ times the approximate $1/T$ behavior of the paramagnetic Tm single-ion susceptibility. This gives a roughly linear intensity increase in temperature below T_2 that turns over to an approximately $1/T$ behavior below T_1, which is qualitatively observed in Fig. 12.

To describe the SRT, we need to understand the reverse effect, the influence of the induced Tm moments on the Fe sites. Using again the dipole field approximation we calculate the effective field created by the Tm $4f$ moments at the Fe sites (J_{4f-3d}). This results in field components that are parallel to the Fe AFM moments used as input in the previous calculations. This demonstrates that the Tm dipole mean-field approximation is insufficient to describe the SRT, as it cannot mediate the $4f$ anisotropy to the Fe sites. It becomes evident that even though a mean-field dipolar field approach describes our data qualitatively correctly, a direct or superexchange interaction between the $3d$ and $4f$ spin systems is required to explain the SRT, in addition to a variation in $4f$ anisotropy.

An additional interesting point is the difference between the temperature dependence of the Fe XMLD and Fe XMCD signals (both taken in reflectivity and total electron yield mode). The Fe XMLD data exhibit an enlarged SRT temperature range. We interpret this as due to fact that the surface behaves differently than the bulk. As to the reason why this is the case, we can only speculate. One reason could be that the surface, even after annealing, contains oxygen vacancies that could affect the magnetic properties. Alternatively, polishing could introduce strain on the nanometer scale; however, strain is usually more problematic in more plastic materials such as metals. The XMCD data would be consistent with a rotation of the FM moment in a narrower temperature range (80–100 K, which is still wider than the range for the bulk FM moment). This could be interpreted in terms of a decoupling of the FM spins from the AFM components, which would be puzzling. Such an interpretation would, however, require that the spectral XMCD shape remains constant during the SRT, which is not the case. Comparing the XMCD spectra at 50 K (Fig. 8) with the one at ∼110 K (inset of Fig. 9), clear gradual changes are observed. This is consistent with moment rotation in magnetic fields of the Mn and Cr in $MnCr_2O_4$ XMCD measured at the $L_{2,3}$ edges in applied field [35]. These results show a clear change in spectral shape when rotating the magnetization. Therefore, an interpretation of the XMCD signal at a given energy in terms of rotation of the FM component would require either a comparison and analysis of the spectral shape in terms of sum rules or a comparison with first-principles calculations, which is beyond the scope of our current paper.

V. CONCLUSION

Detailed resonant x-ray-scattering and absorption experiments are presented on the Fe $L_{2,3}$ edges and the Tm M_5 edge of $TmFeO_3$ in the temperature range of the SRT transition. Clear XMCD and XMLD signals can be observed at the Fe edge, which allow us to separate the FM and AFM components of the Fe moments. Comparing these results with macroscopic magnetization and magnetic neutron-diffraction intensities indicates that the SRT transition of the AFM component occurs continuously, but in a larger temperature range than reported in literature, suggesting that these results describe the magnetic response at the surface. It shows also that in the SRT temperature range the FM component is more complicated to analyze than the AFM component, as it is accompanied with change in spectral shape. An antiferromagnetic Tm moment is observed below T_2 that corroborates these findings. While the occurrence of the Tm spin polarization can be understood in terms of a dipole field approximation in a mean-field approach, the dipolar interaction cannot explain the role of the Tm ions in the SRT. Our results indicate that the $3d-4f$ interaction has a significant nondipolar contribution.

ACKNOWLEDGMENTS

We acknowledge C. A. F. Vaz for carbon coating the sample and F. Nolting for fruitful discussions. We gratefully thank the X11MA, X07MA, and X04SA beamline staff for experimental support. X-ray experiments were performed on the Swiss Light Source and neutron experiments were performed at the Swiss spallation neutron source SINQ, both at the Paul Scherrer Institut (PSI), Villigen, Switzerland. We acknowledge the financial support of PSI, the Swiss National Science Foundation, and its National Center of Competence in Research, Molecular Ultrafast Science, and Technology. E.M.B. acknowledges funding from the European Community's Seventh Framework Programme (FP7/2007-2013) under Grant No. 290605 (PSI-FELLOW/COFUND).

[1] J. A. Leake, G. Shirane, and J. P. Remeika, Solid State Commun. **6**, 15 (1968).
[2] S. M. Shapiro, J. D. Axe, and J. P. Remeika, Phys. Rev. B **10**, 2014 (1974).
[3] H. Pinto, G. Shachar, H. Shaked, and S. Shtrikman, Phys. Rev. B **3**, 3861 (1971).
[4] R. L. White, J. Appl. Phys. **40**, 1061 (1969).
[5] A. K. Zvezdin and V. M. Matveyev, Zh. Eksp. Teor. Fiz. **77**, 1076 (1979).
[6] A. V. Kimel, A. Kirilyuk, A. Tsvetkov, R. V. Pisarev, and T. Rasing, Nature (London) **429**, 850 (2004).
[7] A. V. Kimel, A. Kirilyuk, P. A. Usachev, R. V. Pisarev, A. M. Balbashov, and T. Rasing, Nature (London) **435**, 655 (2005).
[8] S. Baierl, M. Hohenleutner, T. Kampfrath, A. K. Zvezdin, A. V. Kimel, R. Huber, and R. V. Mikhaylovskiy, Nature Photon. **10**, 715 (2016).
[9] T. F. Nova, A. Cartella, A. Cantaluppi, M. Forst, D. Bossini, R. V. Mikhaylovskiy, A. V. Kimel, R. Merlin, and A. Cavalleri, Nat. Phys. **13**, 132 (2017).
[10] N. A. Halasa, G. Depasquali, and H. G. Drickamer, Phys. Rev. B **10**, 154 (1974).
[11] V. P. Plakhty, Yu. P. Chernenkov, and M. N. Bedrizova, Solid State Commun. **47**, 309 (1983).
[12] S. W. Lovesey and S. P. Collins, *X-Ray Scattering and Absorption by Magnetic Materials*, Oxford Series on Synchotron Radiation (Clarendon, Oxford, 1996), Vol. 1.
[13] V. Scagnoli, U. Staub, Y. Bodenthin, M. Garcia-Fernandez, A. M. Mulders, G. I. Meijer, and G. Hammerl, Phys. Rev. B **77**, 115138 (2008).
[14] V. Scagnoli, U. Staub, A. M. Mulders, M. Janousch, G. I. Meijer, G. Hammerl, J. M. Tonnerre, and N. Stojic, Phys. Rev. B **73**, 100409(R) (2006).
[15] T. R. Forrest, S. R. Bland, S. Wilkins, H. C. Walker, T. A. W. Beale, P. D. Hatton, D. Prabhakaran, A. T. Boothroyd, D. Mannix, F. Yakhou, and D. F. McMorrow, J. Phys.: Condens. Matter **20**, 422205 (2008).
[16] S. B. Wilkins, T. R. Forrest, T. A. W. Beale, S. R. Bland, H. C. Walker, D. Mannix, F. Yakhou, D. Prabhakaran, A. T. Boothroyd, J. P. Hill, P. D. Hatton, and D. F. McMorrow, Phys. Rev. Lett. **103**, 207602 (2009).
[17] Y. W. Windsor, M. Ramakrishnan, L. Rettig, A. Alberca, E. M. Bothschafter, U. Staub, K. Shimamoto, Y. Hu, T. Lippert, and C. W. Schneider, Phys. Rev. B **91**, 235144 (2015).
[18] F. Nolting, A. Scholl, J. Stöhr, J. W. Seo, J. Fompeyrine, H. Siegwart, J.-P. Locket, S. Anders, J. Lüning, E. E. Fullerton,

M. F. Toney, M. R. Scheinfein, and H. A. Padmore, Nature (London) **405**, 767 (2000).
[19] L. Le Guyader, A. Kleibert, F. Nolting, L. Joly, P. M. Derlet, R. V. Pisarev, A. Kirilyuk, T. Rasing, and A. V. Kimel, Phys. Rev. B **87**, 054437 (2013).
[20] J. H. Lee, Y. K. Jeong, J. H. Park, M. A. Oak, H. M. Jang, J. Y. Son, and J. F. Scott, Phys. Rev. Lett. **107**, 117201 (2011).
[21] L. Joly, F. Nolting, A. V. Kimel, A. Kirilyuk, R. V. Pisarev, and T. Rasing, J. Phys.: Condens. Matter **21**, 446004 (2009).
[22] C. Y. Kuo, Y. Drees, M. T. Fernandez-Diaz, L. Zhao, L. Vasylechko, D. Sheptyakov, A. M. T. Bell, T. W. Pi, H. J. Lin, M. K. Wu, E. Pellegrin, S. M. Valvidares, Z. W. Li, P. Adler, A. Todorova, R. Kuchler, A. Steppke, L. H. Tjeng, Z. Hu, and A. C. Komarek, Phys. Rev. Lett. **113**, 217203 (2014).
[23] E. Arenholz, G. van der Laan, R. V. Chopdekar, and Y. Suzuki, Phys. Rev. B **74**, 094407 (2006).
[24] S. Czekaj, F. Nolting, L. J. Heyderman, P. R. Willmott, and G. van der Laan, Phys. Rev. B **73**, 020401 (2006).
[25] J. Stöhr, H. A. Padmore, S. Anders, T. Stammler, and M. R. Scheinfein, Surf. Rev. Lett. **5**, 1297 (1998).
[26] U. Staub, V. Scagnoli, Y. Bodenthin, M. García-Fernández, R. Wetter, A. M. Mulders, H. Grimmer, and M. Horisberger, J. Syn. Rad. **15**, 469 (2008).
[27] U. Flechsig, F. Nolting, A. Fraile-Rodríguez, J. Krempaský, C. Quitmann, T. Schmidt, S. Spielmann, and D. Zimoch, AIP Conf. Proc. **1234**, 319 (2010).
[28] V. M. Matveev and V. V. Matveev, Physica B **221**, 408 (1996).
[29] C. Piamonteze, U. Flechsig, S. Rusponi, J. Dreiser, J. Heidler, M. Schmidt, R. Wetter, M. Calvi, T. Schmidt, H. Pruchova, J. Krempasky, C. Quitmann, H. Brune, and F. Nolting, J. Synch. Rad. **19**, 661 (2012).
[30] K. P. Belov, A. K. Zvezdin, A. M. Kadomtseva, and R. Z. Levitin, Usp. Fiz. Nauk **119**, 447 (1976).
[31] G. L. Squires, *Introduction to the Theory of Thermal Neutron Scattering* (Cambridge University Press, New York, 1978), p. 260.
[32] M. Garganourakis, Y. Bodenthin, R. A. de Souza, V. Scagnoli, A. Dönni, M. Tachibana, H. Kitazawa, E. Takayama-Muromachi, and U. Staub, Phys. Rev. B **86**, 054425 (2012).
[33] S. W. Lovesey, E. Balcar, K. S. Knight, and J. Fernández-Rodríguez, Phys. Rep. **411**, 233 (2005).
[34] V. Scagnoli and S. W. Lovesey, Phys. Rev. B **79**, 035111 (2009).
[35] G. van der Laan, R. V. Chopdekar, Y. Suzuki, and E. Arenholz, Phys. Rev. Lett. **105**, 067405 (2010).